Experimental Charge Density Study on an Ionic Crown Ether Complex: [Kc18-Crown-6]$^+N_3^-\cdot H_2O$

T. Koritsanszky,[†] J. Buschmann,[§] P. Luger,*[,§] A. Knöchel,[‡] and M. Patz[‡]

Contribution from the Central Research Institute for Chemistry of the Hungarian Academy of Sciences, H-1525 Budapest, Hungary, Institute of Inorganic and Applied Chemistry, University of Hamburg, D-20146 Hamburg 13, Germany, and Institute for Crystallography, Free University of Berlin, D-14195, Berlin 33, Germany

Received May 24, 1993[⊕]

Abstract: The low-temperature (120 K) structure experimental charge density distribution and electrostatic potential of the title complex were determined from high-resolution X-ray diffraction intensities. The molecular structure and packing is in accord with previous observations on analogous compounds. The nuclear-centered spherical harmonics expansion technique was applied in the treatment of the data to extract the static electron density. Deformation electron density maps in nonbonded regions of the oxygen atoms show lone-pair polarization toward the cation. This valence deformation is compared to that found in the neutral host–guest complex of 18-crown-6·2cyanamide. The anisotropic atomic displacement parameters are tested against the rigid-body motion model, and the residuals for both structures are analyzed with computer graphics. The degree of transferability in the topology of static density deformations is examined in connection with the transferability in the pattern of residual root-mean-square surfaces representing atomic displacements due to internal motion.

Introduction

Macrocyclic polyethers like 18-crown-6 are known to form stable ionic complexes,[1] especially with alkali and alkali earth cations, and nonionic complexes with neutral, acidic guest molecules.[2] An important structural parameter of the macrocation is the position of the metal ion relative to the ring's mean plane. This depends not only on the size of the cation but also on the anion and on the presence of a solvent molecule.[3] Neutral polar guests are usually coordinated via hydrogen bonds. The binary complex (1:2 host:guest stoichiometry) is a typical formation because it enables the dipoles of the guest molecules to be compensated.[4]

The host–guest interactions, such as ion–dipole, dipole–dipole forces, and hydrogen bridges, are expected to take place via the ether oxygen atoms and presumably induce polarization in their valence density as well as in the C–O bonds. Density deformations due to "secondary forces" are close to the observable limit even if high-resolution X-ray diffraction data are available to determine the charge density. The interpretation of the measurement involves the optimization of parameters representing the thermally averaged electron density in the crystal. Shortcomings in this parametrization may lead to high correlations between least-squares variables, those describing asphericities in the valence density and those accounting for nuclear motions. In other words, static density deformations thought to be of chemical relevance could be biased due to the inadequate decomposition of the thermal smearing. The static charge density extracted from X-ray diffraction intensities should be interpreted with caution, especially if large amplitude internal vibration modes have considerable contributions to the smearing. A careful analysis should not neglect, as is frequently done, a test of the anisotropic displacement parameters (ADPs) for their physical significance.

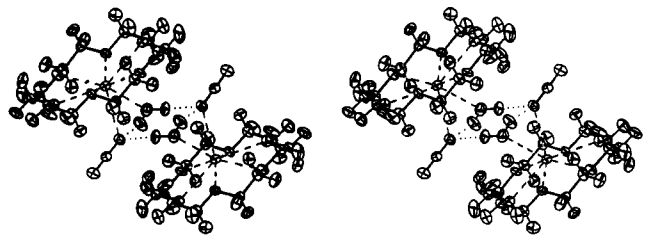

Figure 1. Stereo ORTEP drawing of two [Kc18-crown-6]$^+N_3^-\cdot H_2O$ complexes related by the crystallographic inversion center; thermal ellipsoids at the 70% probability level.

Due to recent improvements in experimental techniques and data processing, it has become evident that the effects of nonbonded interactions on the electron density are indeed observable,[5–8] in spite of the difficulties mentioned above. The results presented in terms of deformation electron density are sometimes conflicting and often of qualitative nature, although extensive studies on α-oxalic acid dihydrate have shown that an excellent quantitative agreement between theory and experiment can be achieved.[9,10] It seems widely accepted that the characteristics of density redistribution, upon forming weak or moderately strong hydrogen bonds, can be interpreted as a result of mutual polarizations of the functional groups involved.[9,11,12] Theoretical calculations have shown that the charge rearrangement along a D—H···A bond path can be well accounted for by a homogeneous electric field directed from the donor (D) to the acceptor (A).[13] In this respect the influence of a cation on the lone-pair density of the acceptor is expected to be analogous to that of a proton in the hydrogen bond.[11,13–15]

In a previous publication we reported an experimental charge density study on a typical neutral complex, 18-crown-6·2NH_2-

* To whom all correspondence should be addressed.
† Hungarian Academy of Sciences.
‡ University of Hamburg.
§ Free University of Berlin.
⊕ Abstract published in *Advance ACS Abstracts*, June 15, 1994.

(1) Pedersen, C. J. *J. Am. Chem. Soc.* **1967**, *89*, 7017.
(2) Pedersen, C. J. *J. Org. Chem.* **1971**, *36*, 1690.
(3) Bajaj, A. V.; Poonia, N. S. *Coord. Chem. Rev.* **1988**, *87*, 55.
(4) Elbasyouny, A.; Brügge, H. J.; von Deuten, K.; Knöchel, A.; Koch, K. U.; Kopf, J.; Melzer, D.; Rudolph, G. *J. Am. Chem. Soc.* **1983**, *105*, 6568–6577.
(5) Stevens, E. D.; Coppens, P. *Acta Crystallogr.* **1980**, *B36*, 1864.
(6) Olovsson, I. In *Electron and Magnetization Densities in Molecules and Crystals*; Becker, P., Ed.; Plenum: New York, 1980; p 831.
(7) Hermansson, K.; Thomas, J. O. *Acta Crystallogr.* **1982**, *B38*, 2555.
(8) Dam, J.; Harkema, S.; Feil, D. *Acta Crystallogr.* **1983**, *B39*, 760.
(9) Krijn, M. P. C. M.; Feil, D. *J. Chem. Phys.* **1988**, *89*(7), 4199.
(10) Schomaker, V.; Trueblood, K. N. *Acta Crystallogr.* **1968**, *B24*, 63.
(11) Hermansson, K.; Lunell, S. *Chem. Phys. Lett.* **1981**, *80*, 64.
(12) Lunell, S. *J. Chem. Phys.* **1984**, *80*(12), 6185.
(13) Feil, D. *Portugal. Phys.* **1988**, *19*, 21.
(14) Hermansson, K.; Thomas, J. O.; Olovsson, I. *Acta Crystallogr.* **1984**, *C40*, 335.

0002-7863/94/1516-6748$04.50/0

Table 1. Crystal Data and Experimental Conditions for $[Kc18\text{-}Crown\text{-}6]^+N_3^-\cdot H_2O$

formula	$C_{12}H_{24}O_6\cdot KN_3\cdot H_2O$	M (g/mol)	363.46
space group	$P2_1/n$	$F(000)$	776
Z	4		

	X-ray	neutron
T (K)	120(1)	119.8(3)
a (Å)	10.192(3)	10.195(2)
b (Å)	8.838(2)	8.857(2)
c (Å)	19.595(4)	19.600(4)
β (deg)	99.66(1)	99.67(2)
V (Å^3)	1740.03	1744.70
d (g/cm^3)	1.387	1.384
cryst dimens (mm)	0.35 × 0.3 × 0.45	1.7 × 0.95 × 3.2
cryst vol (mm^3)	0.038	3.60
λ (Å)	0.710 68	0.844 20
μ (cm^{-1})	3.37	2.24
θ range (deg)	2–50	2–40
$(h,k,l)_{min}$	–19,–6,–34	–14,–12,–26
$(h,k,l)_{max}$	21,15,37	6,2,28
$(\sin\theta/\lambda)_{max}$ (Å^{-1})	1.0636	
scan type	$\omega - 2\theta$	$\omega - 2\theta$
scan width (deg)	$\Delta\omega = 1.26 + 0.40 \tan\omega$	$\Delta\omega = 1.5$
scan rate (deg/min)	1.0–2.4	0.64
orientation refl	31 ($21° < 2\theta < 35°$)	8 ($12° < 2\theta < 40°$)
standard refl	(–2,3,2), (–4,2,7) (1,3,3), (3,–2,8) (6,0,–8), (1,4,–2)	(0,0,4)
NREF[a] (measured)	19 232	4454
NREF[a] (unique)	9095	3379

[a] Number of reflections.

Table 2. Summary of Least-Squares Refinements [$F > N\sigma(F)$]

	spherical atom	multipole	neutron
N	2	3	3
NREF[a]	7490	6814	2359
NVAR[b]	312	434	443
R	0.0661	0.0421	0.109
R_w	0.0309	0.0171	0.117
S	1.97	1.16	8.47

[a] Number of reflections. [b] Number of variables.

CN.[16] The electron distribution of the C–O bonds and the lone-pair density of the oxygen atoms in the crown were shown to be significantly affected by the hydrogen bonds with the cyanamide guests. (We thank Professor H.-B. Bürgi, University of Bern, for calling our attention to the fact that the dipole moment vector of the cyanamide molecule is situated symmetrically with respect to the C–O bonds to O(4) and not to O(1) as stated incorrectly in ref 16 preceding paper. Thus the asymmetries observed in the geometry and in the deformation density of the C(3)–O(4)–C(5) fragment are not simply due to the polarization induced by the guest.) In both the static model and the dynamic Fourier deformation density maps, charge concentrations were found in the nonbonded area of the oxygen acceptors toward the protons.

This work reports the structure and charge density determination of a typical ionic complex, $[Kc18\text{-}crown\text{-}6]^+N_3^-H_2O$, based on X-ray data collected at 120 K. The aim of the study is to see whether density deformations similar to those for the cyanamide complex are detectable also in the macrocation and to find the extent to which density features of the ring are reproducible. In order to check for bias in the static deformation density due to unresolved thermal smearing, the ADPs are tested by the computer graphics program PEANUT,[17] and the results of three measurements for the two structures are compared. The electrostatic potential maps calculated from the experimental static densities for both complexes are also presented.

Diffraction Experiments and Structure Solution

Commercially available 18-crown-6 was purified by reaction with acetonitrile followed by decomposition. The complex was obtained by dissolving 18-crown-6 and the potassium salt in dichloromethane and by adding ether. The crystals were colorless, with melting point 179 °C.

X-ray Measurement

A crystal of approximately spherical shape was fixed in a thin-walled glass capillary and mounted on a Siemens four-circle diffractometer equipped with a nitrogen gas stream cooling device.[18] For data collection, Zr-filtered Mo Kα radiation was used. Six standard reflections were selected and measured every 60 min. In case of an intensity drop larger than 3% for any of the standards, the reflections used in the refinement of the cell parameters were automatically recentered and a new orientation matrix was calculated. This occurred about once every 9 h. For more experimental details, see Table 1. The small linear absorption coefficient and the globular crystal shape justify the neglect of an absorption correction. The merging of the equivalent reflections was done with the XTAL[19] program system, giving an agreement index of 0.0078.

The structure (Figure 1) was solved by the SHELX76[20] program. All hydrogen atoms could be located by difference Fourier synthesis. The conventional least-squares refinement, minimizing the residual $\sum_H w_H\{|F_{obs}(H)| - k|F_{cal}(H)|\}^2$ with statistical weight $w = 1/\sigma^2(|F_{obs}(H)|)$, was stable and led to the agreement indices listed in Table 2. Relativistic Hartree–Fock scattering factors corrected for anomalous dispersion[21] were used.

Neutron Measurement

The data were collected at the high flux reactor of the Institute Laue-Langevin in Grenoble, France, on the D9 four-circle single-crystal diffractometer with offset χ-circle equipped with a closed-cycle, two-stage DISPLEX cryostat and a one-reflection area detector. The large-size crystals turned out to be sensitive to strain induced by cooling. Therefore, the rather small crystal, which finally served for the experiment was wrapped in aluminum foil before mounting. In the higher scattering angle range, only the 400 strongest reflections in one quadrant of the reciprocal space were measured. An analytical absorption correction was applied with a Gaussian grid integration.[22] Although the internal R-value for merging 1750 replicate measurements was fairly low (0.034), the rather high statistical variation in the intensity-control reflection ($I_{av}(004) = 1972(53)$) indicated instability in the data collection. The structure refinement did not lead to a satisfactory fit, as indicated by the high reliability factors in Table 2. Many reflections with low indices (–2,–1,2; 2,–1,–2; 1,–1,–5; –1,–1,5; –6,0,8) show a severe extinction effect (F_c correction factor of about 0.8) that could not be properly accounted for by the models applied.[23] The geometrical parameters obtained are in fair agreement with those of the X-ray measurement, but the high standard deviations do not allow a quantitative comparison, and thus the result is not interpreted in any further detail.

(15) Olovsson, I.; Ptasiewicz-Bak, H.; McIntyre, G. J. *Z. Naturforsch.* **1993**, *48a*, 3.
(16) Koritsanszky, T.; Buschmann, J.; Denner, L.; Luger, P.; Knöchel, A.; Haarich, M.; Patz, M. *J. Am. Chem. Soc.* **1991**, *113*, 8388–8398.
(17) Hummel, W.; Hauser, J.; Bürgi, H.-B. *J. Mol. Graphics* **1990**, *8*, 214.
(18) Dietrich, H.; Diercks, H. *Messtechnik* **1970**, *78*, 184.
(19) *XTAL2.2 User's Manual*; Hall, S. R., Stewart, J. M., Eds.; University of Western Australia and University of Maryland: Nedlands, WA and College Park, MD, 1987.
(20) Sheldrick, G. M. *SHELX76: A Program for Crystal Structure Determination*; University of Cambridge: England, 1976.
(21) *International Tables for X-ray Crystallography IV*; Ibers, J. A., Hamilton, W. C., Eds.; The Kynoch Press: Birmingham, England, 1974; pp 72–73, 102, 149.
(22) Coppens, P.; Hamilton, W. C. *Acta Crystallogr.* **1970**, A26, 71.
(23) Becker, P.; Coppens, P. *Acta Crytallogr.* **1974**, *A30*, 128; 148.
(24) Hansen, N. K.; Coppens, P. *Acta Crystallogr.* **1978**, *A34*, 909.

Table 3. Multipole Populations and Radial Screening Constants for [Kc18-Crown-6]$^+N_3^-\cdot H_2O$[a]

		18-crown-6				N_3^-			H_2O	
		O(1)	C	O(4)	H	N(19)	N(20)	N(21)	O(w)	H(w)
κ		0.94(2)	0.98(2)	0.94(2)	1.0	0.91(2)	1.02(2)	1.02(2)	0.95(2)	1.0
1	m									
0	0	6.43(3)	4.22(3)	6.45(3)	0.78(2)	6.65(8)	4.41(8)	4.94(8)	6.46(7)	0.77(5)
1	1	−0.04	−0.12	−0.02		0.31	0.55	0.19		
	−1	−0.07	−0.06	−0.05		0.06				
	0			−0.07	0.11	−0.05		0.07	0.14	0.18
2	0	0.02	0.06			−0.26		0.05	0.07	
	1	0.02					−0.08			
	−1			−0.02			−0.07	0.07		
	2	0.02	−0.10			0.38		−0.05	−0.10	
	−2	−0.02	0.03			0.05		−0.04		
3	0			−0.01		0.04			−0.14	
	1	−0.02	−0.18			−0.25	−0.14			
	−1	−0.02	−0.23	−0.02		−0.03				
	2					−0.07			0.09	
	−2	−0.01		−0.02		0.05		−0.06		
	3	0.13	0.25	0.14		0.23	0.12	0.04		
	−3	0.02	0.12	0.04			0.06	−0.03		
4	0		0.05			0.13	−0.07	−0.04		
	1									
	−1	0.01					−0.03			
	2		−0.05	−0.03		−0.08	0.14	0.04	0.05	
	−2		0.13	0.03			−0.06	−0.05		
	3	0.03		0.02						
	−3			−0.02		−0.06	0.08	−0.10		
	4		0.05	0.02		0.10	−0.12		0.04	
	−4			0.02						
	σ_{max}	0.018	0.009	0.017	0.004	0.035	0.033	0.037	0.031	0.021

[a] The errors for the atomic charges and radial screening constants are explicitly specified, but only the significant multipole populations ($P_{lm} > \sigma(P_{lm})$) are given. The maximum values of the standard deviations (σ_{max}) are also indicated.

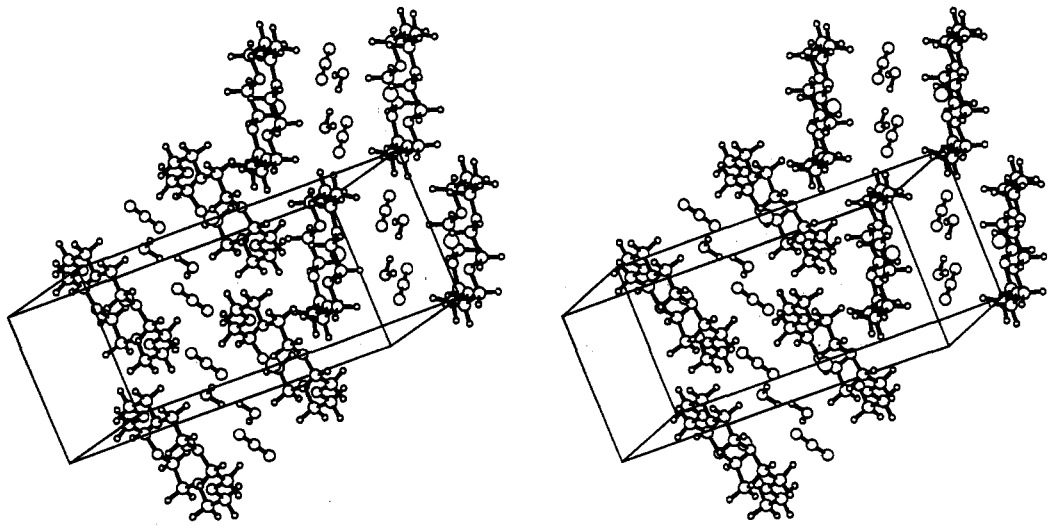

Figure 2. Molecular packing of [Kc18-crown-6]$^+N_3^-\cdot H_2O$ generated by SCHAKAL.[46]

Multipole Refinement

After the conventional treatment of the X-ray data, the aspherical-atom scattering formalism[24,25] was applied. In the crown ether the atomic-site coordinate systems, the radial functions[26] and the local-site symmetries were chosen to be the same as those in our previous study.[16] For the carbon and oxygen atoms, the x and y axes were selected in the plane defined by the atom in question and its two neighbors. For the carbon atoms, a local mirror symmetry (in the xy plane) was imposed. Due to the asymmetry in the oxygen–potassium coordination, one cannot ignore differences between the valence deformation densities of the oxygen atoms situated above and below the mean plane of the crown. Therefore, the oxygen atoms were constrained in two groups of three to have the same valence density. These considerations led to one carbon, two oxygen, and one hydrogen atom in the crown to be described independently. The potassium cation was represented only by its core density, and no charge transfer between the host and the guests or between the guests was allowed. No symmetry restrictions were applied to the azide anion, but for the water molecule, $mm2$ symmetry was maintained. The non-hydrogen atoms were described up to the hexadecapolar level in the multipole expansion.

The simultaneous refinement of the multipole populations and the conventional variables of the hydrogen atoms usually leads to highly correlated shifts. Due to the electroneutrality constraint, all variables are affected by the indeterminacy in the charges of the hydrogen atoms. To overcome this problem, the following

(25) Koritsanszky, T. *LSMOL: Multipole Refinement Program, SDP version*; State University of New York: Buffalo, NY, 1987.
(26) Clementi, E.; Raimondi, D. L. *J. Chem. Phys.* **1963**, *33*, 2686.

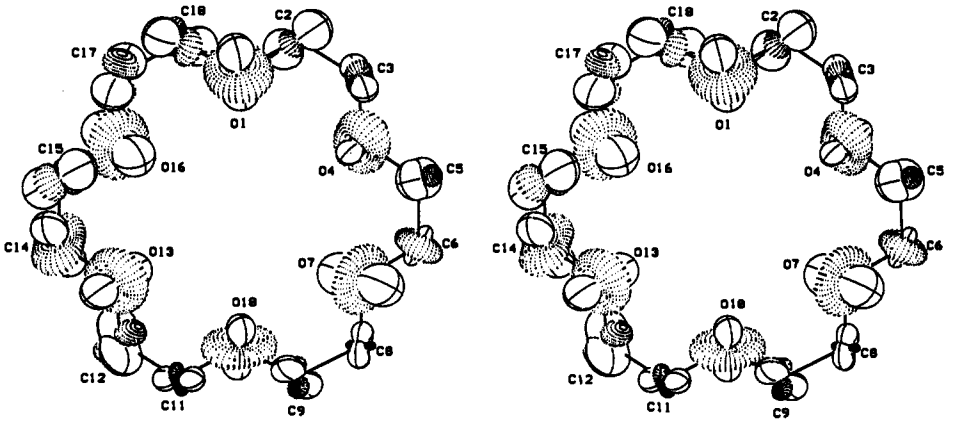

Figure 3. PEANUT stereo plot of the crown ether ring in $[Kc18\text{-crown-}6]^+N_3^-\cdot H_2O$ showing the residual root-mean-square displacement surfaces not accounted for by the rigid-body model. $\Delta U = U_{obsd}(X\text{-ray}) - U_{calcd}(TLS)$.

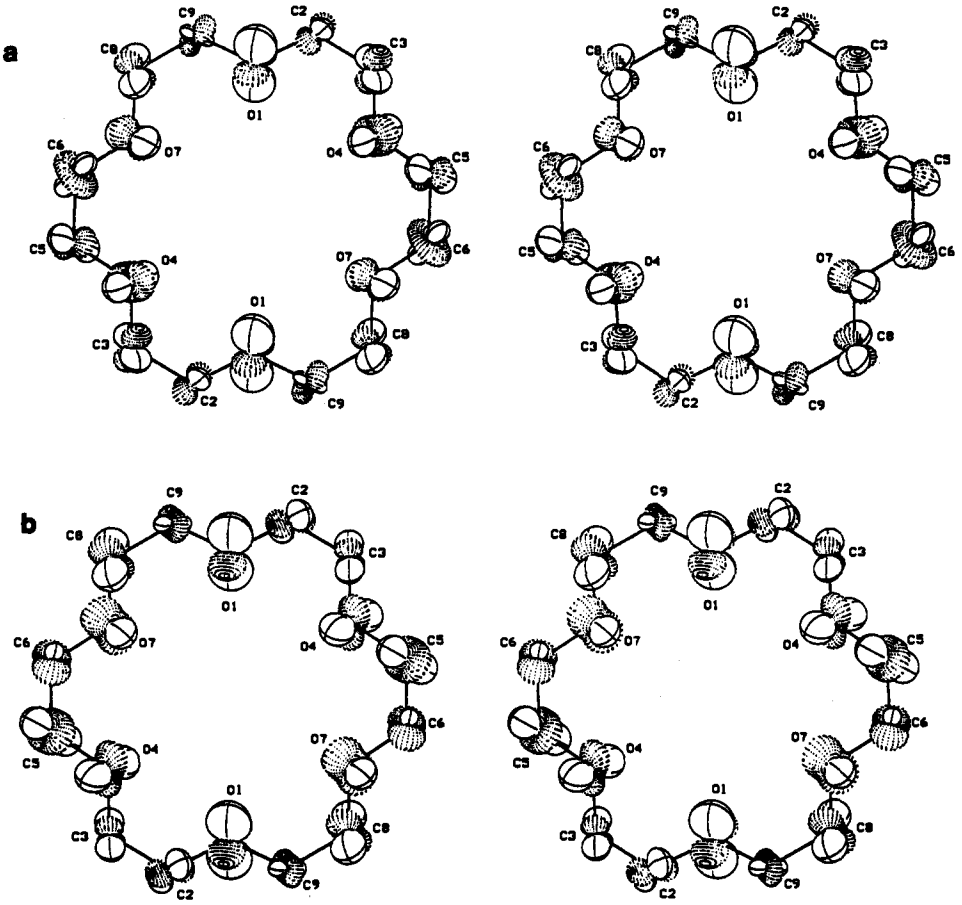

Figure 4. PEANUT stereo plot of the crown ether ring in $18\text{-crown-}6\cdot 2NH_2CN$ showing the residual root-mean-square displacement surfaces not accounted for by the rigid-body model. (a) $\Delta U = U_{obsd}(neutron) - U_{calcd}(TLS)$. (b) $\Delta U = U_{obsd}(X\text{-ray}) - U_{calcd}(TLS)$.

strategy was applied. An initial set of isotropic thermal parameters of the hydrogen atoms was obtained by the spherical-model refinement on the low-order X-ray data and used in the multipole refinement. In the next step, ADPs of the hydrogen atoms were estimated by fitting the rigid-body model to the motion of the non-hydrogen atoms, and these estimated values were fixed during the refinement of charge density and all other conventional parameters. The correctness of this estimation was judged by the reasonableness of the C–H bond distances and by the net atomic charges of the hydrogen atoms obtained after the refinement. In order to improve the reliability of the charge density of the water molecule, the neutron parameters of the hydrogen atoms (H(w1), H(w2)) were used and kept fixed during the refinement. The density asphericity of a hydrogen atom was represented by a bond-directed dipole, for which the population was refined together with the charge and the positional parameters. The contracted function given by Stewart[27] was used as the monopole scattering factor. The indices of fit of the different refinements are listed in Table 2 and the multipole parameters in Table 3.

Molecular Geometry and Packing

The molecular data of interest are given in Table 4. The C–C bond distances are uniformly 1.505(1) Å, and for the C–O distances, only a slight deviation from the average value of 1.422(1) Å is established. The spherical refinement gives considerably shorter C–C (1.495(2) Å) and a bit longer C–O (1.427(2) Å)

(27) Stewart, R. F.; Davidson, E. R.; Simpson, W. T. *J. Chem. Phys.* **1965**, *42*, 3175.

Table 4. Bond Distances (Å), Bond Angles (deg), and Torsion Angles (deg) for [Kc18-Crown-6]$^+N_3^-\cdot H_2O$[a]

atoms A	B	C	D	distance B–C	angle A–B–C	torsion angle A–B–C–D
C(18)	O(1)	C(2)	C(3)	1.419(1)	111.3(1)	−175.4(1)
O(1)	C(2)	C(3)	O(4)	1.505(1)	108.6(1)	67.8(1)
C(2)	C(3)	O(4)	C(5)	1.424(2)	108.6(1)	178.6(1)
C(3)	O(4)	C(5)	C(6)	1.421(2)	110.9(1)	177.9(1)
O(4)	C(5)	C(6)	O(7)	1.505(1)	109.2(1)	−64.5(1)
C(5)	C(6)	O(7)	C(8)	1.418(1)	108.3(1)	−172.2(1)
C(6)	O(7)	C(8)	C(9)	1.421(2)	112.5(1)	−179.4(1)
O(7)	C(8)	C(9)	O(10)	1.505(2)	108.9(1)	64.8(1)
C(8)	C(9)	O(10)	C(11)	1.425(1)	109.2(1)	176.8(1)
C(9)	O(10)	C(11)	C(12)	1.429(1)	110.7(1)	173.5(1)
O(10)	C(11)	C(12)	O(13)	1.505(2)	109.0(1)	−67.8(1)
C(11)	C(12)	O(13)	C(14)	1.422(2)	108.7(1)	−177.7(1)
C(12)	O(13)	C(14)	C(15)	1.420(2)	111.8(1)	−177.8(1)
O(13)	C(14)	C(15)	C(16)	1.505(2)	108.3(1)	64.6(1)
C(14)	C(15)	O(16)	C(17)	1.423(1)	108.2(1)	170.7(1)
C(15)	O(16)	C(17)	C(18)	1.423(2)	111.8(1)	−177.9(1)
O(16)	C(17)	C(18)	O(1)	1.505(1)	108.8(1)	−64.7(1)
C(17)	C(18)	O(1)	C(2)	1.420(2)	109.0(1)	−178.1(1)
N(19)	N(20)	N(21)		1.178(1)	179.8(2)	
	N(19)	N(20)	N(21)	1.181(1)		
	N(19)	H(w2)	O(w)	2.029(1)	151.1(3)	
	N(19)	H(w1)	O(w)′	1.992(1)	173.6(3)	
H(w1)	O(w)	H(w2)		0.920(3)	104.1(4)	104.1(4)
H(w2)	O(w)	H(w1)		0.984(3)		

[a] Entries are based on the multipole refinement. Positions of H(w1) and H(w2) were fixed at the neutron values.

Table 5. Interatomic ($K^+\cdots X$) Distances (Å) and ($X\cdots K^+\cdots Y$) Angles (deg) for the Coordination of the Cation[a]

atoms A···B···C	distance A···B	angle ABC	atoms A···B···C	distance A···B	angle ABC
O(1)···K···O(4)	2.893	58.2	O(4)···K···O(7)	2.956	58.6
O(7)···K···O(10)	2.780	58.8	O(10)···K···O(13)	2.973	58.1
O(13)···K···O(16)	2.908	57.3	O(16)···K···O(1)	2.926	58.0
O(w)···K···N(19)	2.880	59.6	N(19)···K	2.896	

[a] Estimated standard deviations are 0.001 for the distances and 0.1 for the angles.

Table 6. Libration (L), Translation (T), and Screw (S) Tensors in the Cartesian Crystal System[a]

L (rad²)			l	T (Å²)			t
1(2)	0(6)	0(8)	5	146(7)	12(6)	−12(7)	200
	4(2)	−1(1)	4		161(7)	−17(9)	154
		5(9)	1			185(20)	139

S (rad Å)		
0(1)	−1(2)	−1(1)
0(2)	−1(1)	−2(1)
−1(1)	1(1)	1(1)

$R = 0.1385$

[a] Entries are multiplied by 10^4. l and t are the eigenvalues.

average bond distances. The average C–H bond distance (1.080(7) Å) obtained by the multipole refinement is closer to the expected value (1.098 Å) than is that based on the conventional model (0.965(15) Å).

The ring can be described as (ap,sc,ap) conformation at all of the six O–C–C–O segments, which corresponds to an approximate D_{3d} symmetry. The distances of the oxygen atoms from the ring's least-squares plane are 0.240(1), −0.242(1), 0.173(1), −0.246(1), 0.213(1), −0.117(1) Å for O(1), O(4), O(7), O(10), O(13), and O(16), respectively. The potassium atom, due to its 8-fold coordination (to O(1)–O(16), to N(19), and to O(w)), is displaced by 0.770(1) Å away from the mean plane of the crown (Figure 2). The similarity of the different K···O and K···N distances, which are in the range of 2.780(1)–2.973(1) Å (Table 5), indicates

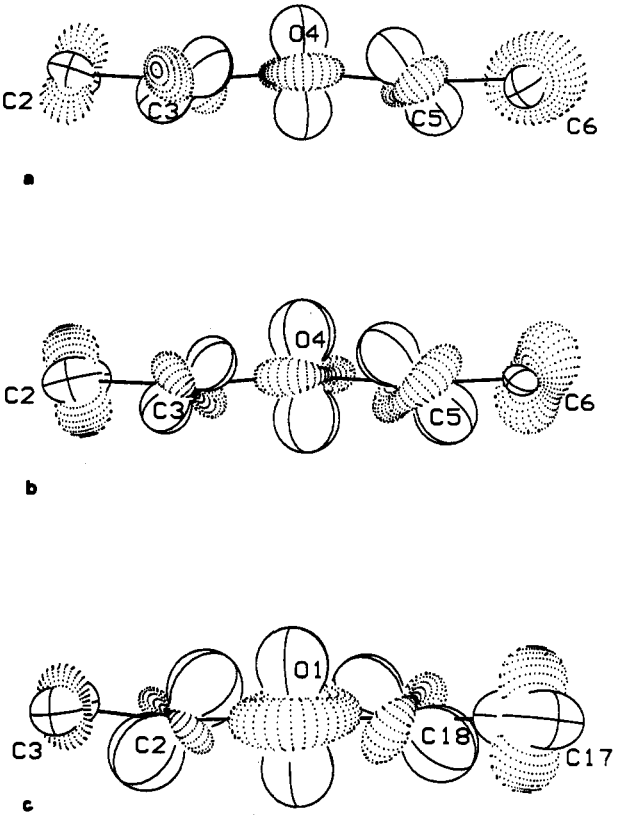

Figure 5. PEANUT stereo plot displaying the residual root-mean-square displacement surfaces of C–C–O–C–C fragments viewed along the C–O–C bisector. (a) Neutron for 18-crown-6·2NH_2CN. (b) X-ray for 18-crown-6·2NH_2CN. (c) X-ray for [Kc18-crown-6]$^+N_3^-\cdot H_2O$.

a balance in the attractive forces acting between the cation and the surrounding ligating atoms.

Two anions are linked by two water molecules via hydrogen bonds (N···H(w1)—O(w)—H(w2)···N′···H(w1)′—O(w)′—H(w2)′···N) in such a way that the atoms are arranged nearly in a plane and clustered between two crown ethers (Figure 1). The geometrical parameters of the hydrogen bonds (Table 4) indicate intermediate strength.

Thermal Motion Analysis

The atomic thermal motion of the 18-crown-6 was analyzed by adjusting a translation, a libration, and a screw-rotation tensor of the rigid-body motion model[28,29] to the anisotropic displacement parameters obtained by the multipole refinement (Table 6). As it appears, the librational component does not make a significant contribution to the vibrational motion of the molecule. The overall fit is poor in comparison to that obtained for 18-crown-6·2cyanamide for both observations ($R_n = 0.0972$, $R_x = 0.1021$), which may be due either to the higher observation to variable ratio or to a more intense internal motion.

The physical significance of the thermal parameters can be judged by inspecting the residual root-mean-square displacement (RMSD) surfaces defined in the following way:

$$\langle \Delta\mu^2(\mathbf{n}) \rangle^{1/2} = (\mathbf{n}'\Delta\mathbf{U}\mathbf{n})^{1/2}$$

where $\mathbf{n}$ is a unit vector in any direction and $\mathbf{U}$ is the atomic displacement tensor. The residual ADPs are the differences between those obtained by the final refinement and those predicted by the rigid-body model ($\Delta\mathbf{U} = \mathbf{U}_{obsd} - \mathbf{U}_{calcd}(TLS)$). The corresponding RMSD surfaces displayed by the computer graphics

(28) Krijn, M. P. C. M.; Graafsma, H.; Feil, D. *Acta Crystallogr.* **1988**, *B44*, 609.
(29) Koritsanszky, T.; Bürgi, H.-B. *UBSBA: University Bern Segmented Body Analysis Program*; University Bern: Bern, Switzerland, 1992.

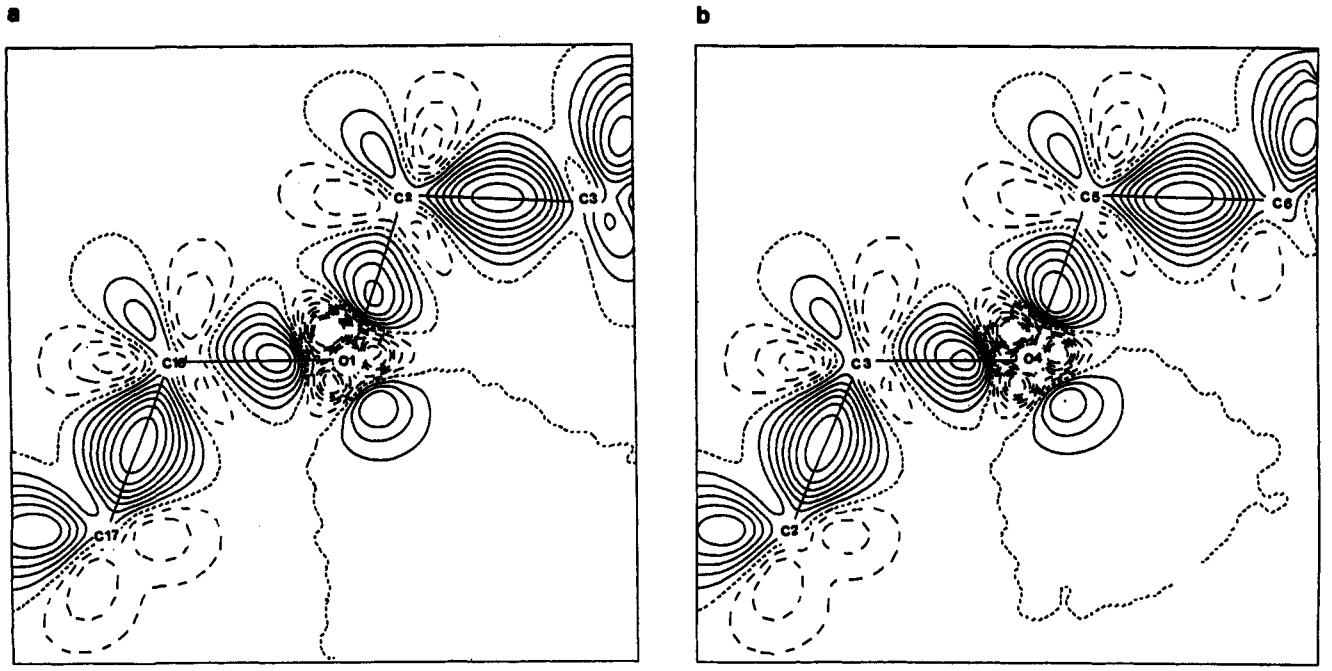

Figure 6. Multipole model deformation electron density sections for $[Kc18\text{-crown-}6]^+N_3^-\cdot H_2O$. (a) C(18)–O(1)–C(2) plane. (b) C(3)–O(4)–C(5) plane. Contour intervals are 0.05 e/Å^3; charge excess, solid line; depletion, dotted line; zero level, dashed line.

program PEANUT are seen in Figure 3. The positive (real) parts of the surfaces (outlined) at the oxygen atoms are perpendicular to the corresponding C–O–C plane in which the negative (imaginary) areas (dotted) are situated. It means that the motion perpendicular to the C–O–C plane is underestimated while the in-plane motion is overestimated by the rigid-body model. This pattern could be interpreted as the result of a large amplitude motion of the oxygen atoms due to torsional libration about the C–C bonds. A recent study on the vibrational modes of 18-crown-6 established that the vibrations of very low wavenumbers (<70 cm^{-1}) can indeed be assigned to the out-of-plane modes of the ring of both D_{3d} and C_i conformations.[30]

Figures 4a and 4b display residual RMSD surfaces for 18-crown-6·2 cyanamide that correspond to the neutron and the X-ray multipole thermal parameters, respectively. The comparison shows a high degree of similarity in terms of arrangements and orientations of the surfaces. This is in good agreement with our previous observation that the 25% difference in the ADPs obtained by the two diffraction techniques can be accounted for by the translational component of the rigid-body motion.

The similarity obtained for the two structures by three independent measurements is encouraging. A more detailed comparison is made in Figure 5, where the residual RMSD surfaces, obtained from the three experiments for the two complexes, are displayed for a C–C–O–C–C fragment viewed along the C–O–C bisector. The approximate *mm*2 symmetry is clearly recognizable. The surfaces are isotropically extended for the atoms in the ionic crown ether, which can be attributed to the 20 K higher temperature of the data collection.

Deformation Electron Density

The charge rearrangement due to bond formation is interpreted in terms of standard deformation density maps with the promolecular reference density. The total electron density is provided by the multipole model distribution fitted to the X-ray data. Sections in the planes containing the two "independent" C–O–C fragments are displayed in Figure 6. A considerable topological similarity and even a certain quantitative agreement exists between the title structure and the neutral cyanamide crown complex when the corresponding sections are compared. The average heights of the C–C bond peaks are 0.73 and 0.75 e/Å^3 for the neutral and ionic complexes, respectively. The same comparison for the C–O bonds shows larger deviations (0.37, 0.52 e/Å^3). In the title compound, the C–O–C units exhibit the bisecting mirror symmetry, i.e., approximately equal bond peaks are visible. The strengthening of the C–O bond maxima relative to those observed for the neutral complex is accompanied by the weakening of the lone-pair peaks in the C–O–C plane.

The deformation electron density in the planes bisecting the C–O–C angles at the O(1) and O(4) atoms (Figure 7) shows a contiguous lobe with its maximum shifted in the direction of the cation. This lone-pair density is very similar to that obtained for those oxygen atoms in 18-crown-6·2 cyanamide that are involved in hydrogen bonding (O(1), O(7)).

Theoretical model calculations on some metal hydrates (Li^+, Mg^{2+}, Be^{2+}, and Al^{3+})[31] have demonstrated that the influence of the cation on the water molecule is primarily a polarization effect. In the O–H bonds and in the outer region of the lone pair of the oxygen atom, the interaction density (calculated with reference to the isolated monomers) revealed a significant charge excess at the expense of charge in close vicinity to the nuclei. The latter deficiency cannot be observed by X-ray diffraction, but the extension and rearrangement of the lone-pair density of the oxygen atom has already been detected experimentally. For example, in $[Co^{2+}(H_2O)_6]$[32] and in $[Ni^{2+}(H_2O)_6]$,[33] the arrangement of the nonbonded density was shown to be correlated with the coordination of the corresponding oxygen atoms. There was found an overall tendency for the lone-pair density to be formed as a single peak in the case of a trigonal coordination (sp^2) and as a double-peak for a tetrahedral surrounding (sp^3). These findings cannot directly be adapted to a more complex case of the crown ether, mainly because of its ring structure and the expectation that the C–O–C moiety is less polarizable than the water molecule. The metal–oxygen distance, the degree of covalence, the type of the cation, and the crystal field can also considerably influence the final picture.

(30) Fukuhara, K.; Keda, K.; Matsusura, H. *J. Mol. Struct.* **1990**, *224*, 203.

(31) Hermansson, K.; Olovsson, I.; Lunell, S. *Theor. Chim. Acta* **1984**, *64*, 265.

(32) Kellersohn, T.; Delaplane, R. G.; Olovsson, I.; McIntyre, G. J. *Acta Crystallogr.* **1993**, *B49*, 179.

(33) Ptasiewicz-Bak, H.; Olovsson, I.; McIntyre, G. J. *Acta Crystallogr.* **1993**, *B49*, 192.

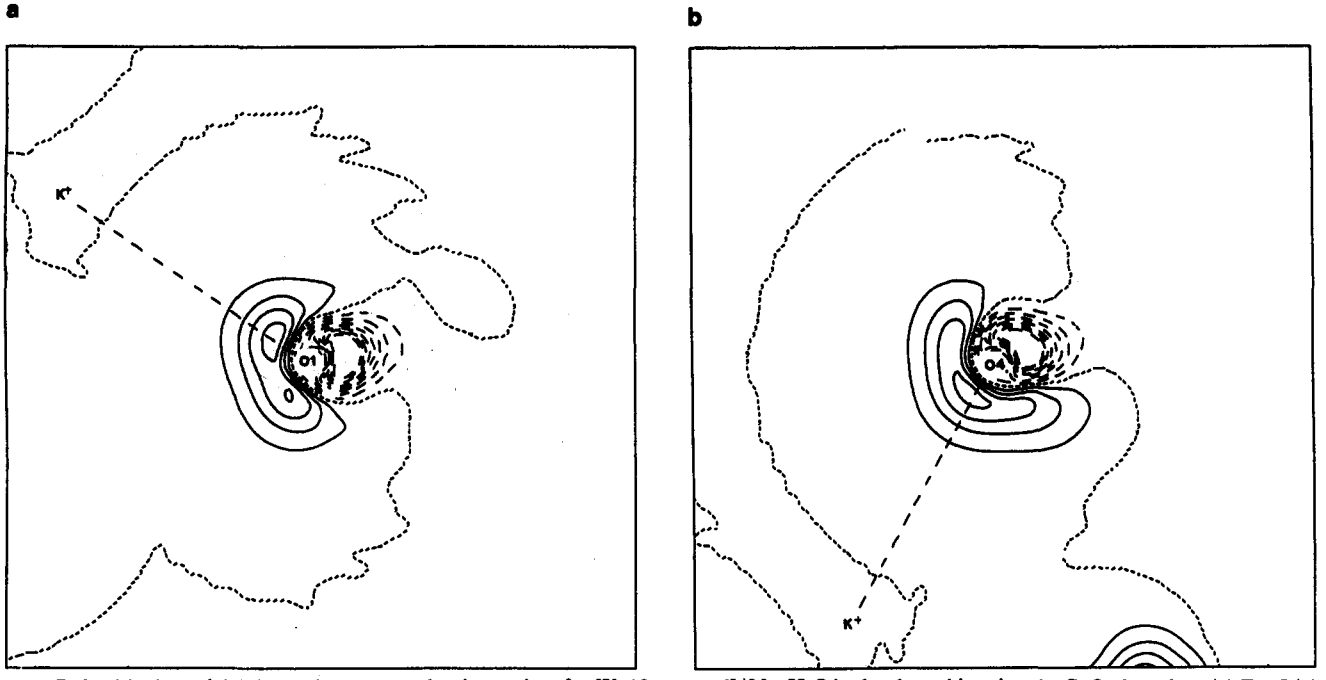

Figure 7. Multipole model deformation electron density sections for $[Kc18\text{-crown-}6]^+N_3^-\cdot H_2O$ in the planes bisecting the C–O–C angles. (a) For O(1). (b) For O(4). Contours are the same as in Figure 6.

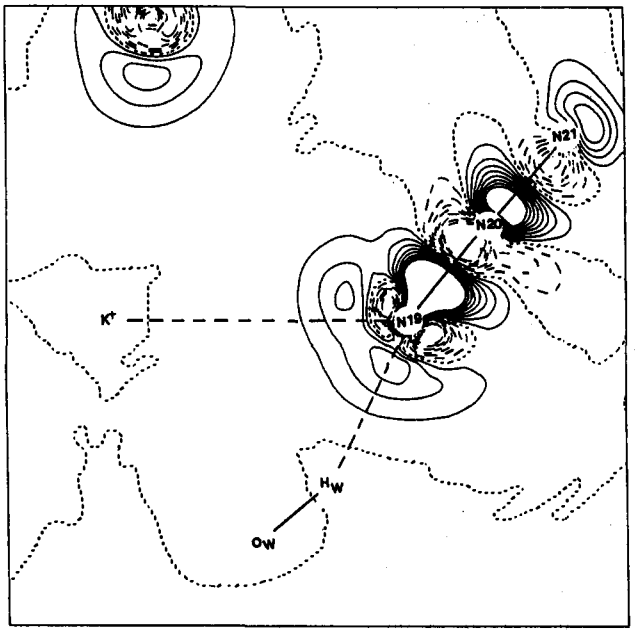

Figure 8. Multipole model deformation electron density of the azide molecule in the plane defined by the K^+, N(19), and N(20) atoms. The projection of the O(w)–H(w) bond is also indicated. Contours are the same as in Figure 6.

The deformation density of the azide anion in the complex (Figure 8) differs considerably from those obtained for NaN_3[34] and KN_3[35] due to different crystal fields. In those structures, the anion is in a special position of high symmetry (3*m* for NaN_3 and *mmm* for KN_3). For NaN_3, a structure refinement based on third-order cumulant expansion led to a triangular-shaped lone-pair deformation with the density maxima extending toward the cations. The azide anion in the title complex shows similar features, since the three maxima found in the lone-pair region of N(19) are located in the direction of the cation and of the two nearby hydrogen atoms of the water molecules (only one of the O(w)—H(w)···N(19) bridges is seen in Figure 8). The charge concentration at this terminal nitrogen atom makes the N(19)–N(20) bond very polarized, and thus the terminal lone pairs of N(19) and N(21) are very different from each other.

Electrostatic Potential

A quantitative characterization of the chemical behavior of a molecule or a certain group of atoms is provided by the electrostatic potential, which reliably predicts those regions of the system where electrophilic or nucleophilic attacks are most likely to occur. This function is of special interest for the complexes being described here since it gives a measure and a detailed mapping of the intermolecular forces responsible for the complexation.

Different procedures have been proposed for extracting electronic properties from X-ray diffraction data. A thermal average of the potential can directly be resolved from the structure factors via a Fourier summation,[36-38] or, alternatively, the corresponding static function can be derived from the model density fitted to the observations.[39,40] The latter approach has been realized in many applications,[41,42] although in most cases only the monopole contribution has been considered.[43,44] The result presented here is based on the method of Su and Coppens,[45] a formalism which allows electrostatic properties to be expressed in terms of the multipole populations of the individual pseudo-atoms.

Figure 9 shows the relief plots of the electrostatic potential for the macrocation (Figure 9a) and for the crown ether (Figure 9b)

(34) Stevens, E. D.; Hope, H. *Acta Crystallogr.* **1977**, *A33*, 723.
(35) Stevens, E. D.; Rys, J.; Coppens, P. *J. Am. Chem. Soc.* **1977**, *99*, 265.
(36) Bertaut, E. F. *J. Phys. Chem. Solids* **1978**, *39*, 97.
(37) Stewart, R. F. *Chem. Phys. Lett.* **1979**, *65*, 335.
(38) Schwarzenbach, D.; Thong, N. *Acta Crystallogr.* **1979**, *A35*, 652.
(39) Spackman, M.; Stewart, R. F. In *Chemical Applications of Atomic and Molecular Electrostatic Potentials*; Politzer, P., Truhlar, D. G., Eds.; Plenum Press: New York, London, 1981.
(40) Epstein, J.; Swanton, D. J. *J. Chem. Phys.* **1982**, *77*, 1048.
(41) He, X. M.; Swaminathan, S.; Craven, B. M.; McMullan, R. K. *Acta Crystallogr.* **1988**, *B44*, 271.
(42) Destro, R.; Bianchi, R.; Morosi, G. *J. Phys. Chem.* **1989**, *93*, 4447.
(43) Lecomte, C.; Souhassou, M.; Ghermani, N.; Pichon-Pesme, V.; Bouhmaida, N. In *Studies of Electron Distributions in Molecules and Crystals*; Transactions of the American Crystallographic Association 26; Blessing, R., Ed.; American Crystallographic Association: Pittsburgh, PA, 1990.
(44) Ghermani, N.; Bounmaida, N.; Lecomte, C. *Acta Crystallogr.* **1993**, *A49*, 781.
(45) Su, Z.; Coppens, P. *Acta Crystallogr.* **1992**, *A48*, 188.
(46) Keller, E. *SCHAKAL88. Graphics program for molecular and crystallographic models*; Albert-Ludwigs-Universität: Freiburg, Germany, 1988.

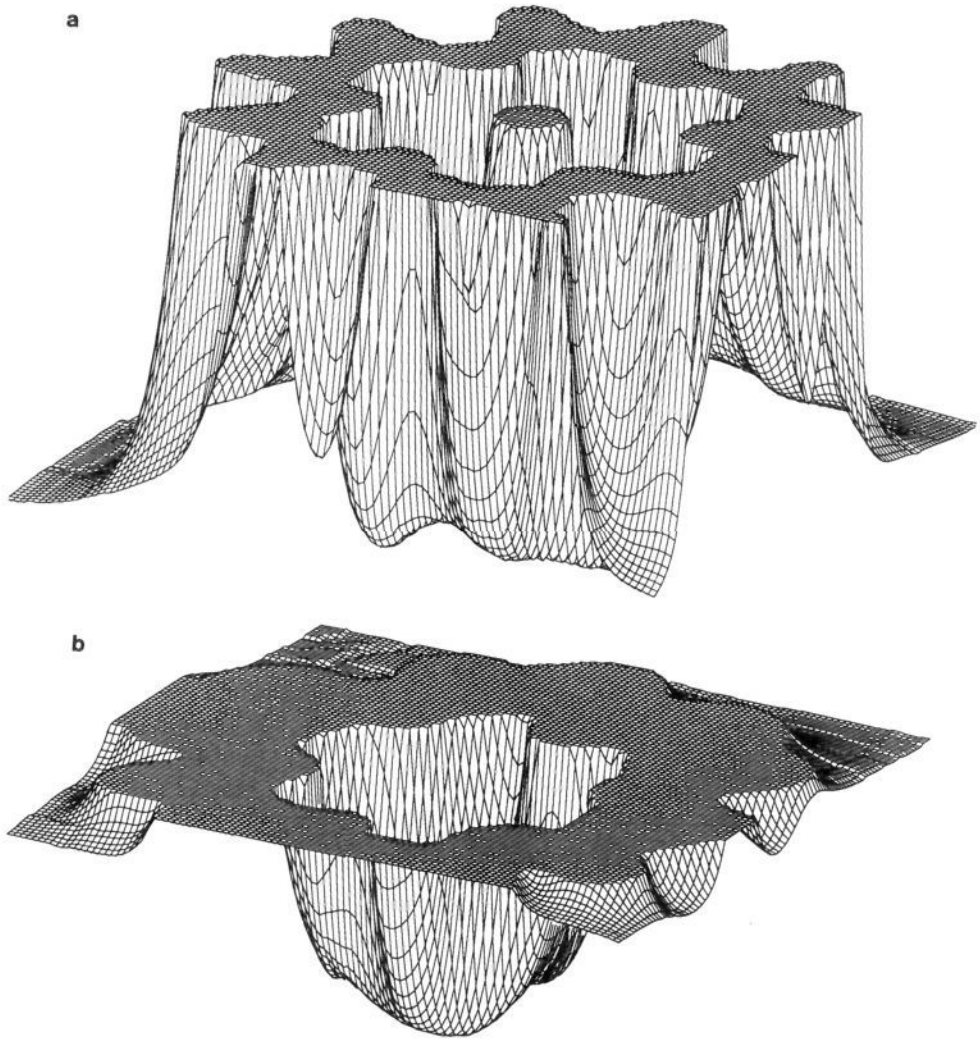

Figure 9. Relief maps of the electrostatic potential in the least-squares plane of the 18-crown-6 ring for the ionic complex. (a) The contribution of the potassium ion is included (peaks are cut at 1.0 e/Å). (b) The "free" ring as extracted from the crystal environment (the positive peaks are cut at 0.1 e/Å).

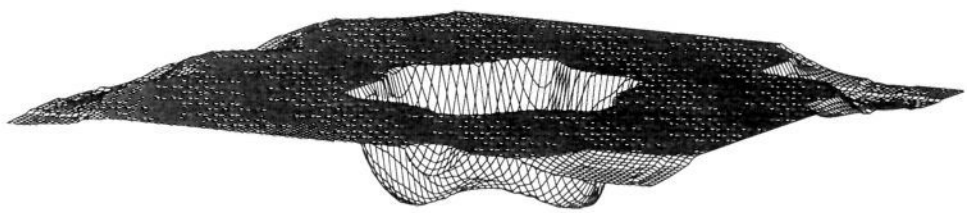

Figure 10. Relief map of the electrostatic potential in the least-squares plane of the 18-crown-6 ring for the neutral complex.

isolated from the crystal structure of the title compound. The maps are generated for the least-squares plane through the ring atoms and include the contributions of all pseudoatomic densities, up to the highest actual level of the multipole expansion. The macrocation is electropositive, with a "ring-shaped" potential minimum of 0.07 e/Å located around the potassium. The peaks are cut at 1 e/Å for a clear visibility. The negative range of the potential for the isolated polyether ring (without the contribution of the K^+ atom) forms a well-defined cavity (Figure 9b) with a minimum of –0.35 Å. The area enclosed in the negative surface represents the reduced potential for a positive charge. The positive peaks are cut at 0.1 e/Å level. This topology is to be compared with that obtained for the neutral 18-crown-6 in the corresponding plane (Figure 10). Both maps visualize the form of the cavity where the cation is to be captured, but for the neutral compound the negative basin is less extended and flatter than that found for the isolated molecule in the ionic structure. This comparison clearly reveals the polarization induced by the cation on the field of the ring in the macrocation.

Concluding Remarks

In the ionic complex, the D_{3d} symmetry of the polyether ring is maintained to a good approximation by the cation coordinated close to the center of the ring. This structural aspect is revealed in the deformation electron density, since peaks of comparable height and shape were found for the different C–O bonds and similarly for the lone pairs of the corresponding oxygen atoms. The nonbonding deformation density of the oxygen atoms is topologically equivalent to those obtained for oxygens that are involved in hydrogen bonds in 18-crown-6·2 cyanamide. These contiguous lobes with the maxima situated nearly on the O···K^+ internuclear vectors are likely to be formed on account of the electrostatic interactions between the atoms considered. The lone-

pair polarization toward the proton in the neutral complex and toward the potassium in the macrocation is in qualitative agreement with previous calculations and diffraction experiments on hydrogen-bonded water molecules.

The C–C bond density in the ring is almost perfectly transferable from one 18-crown-6 compound to the other. This is not true for the C–O bonds, as the valence deformation at the oxygen atoms was found to be strongly affected by secondary forces.

The transferability shown in the residual ADPs is of foremost significance. The same pattern of the RMSD surfaces was obtained from different diffraction data and for both molecules in spite of the considerable differences in the corresponding ADPs. This may indicate that the "asphericity bias" in the conventional least-squares variables is minimized.

The electrostatic potential obtained from the model density of both compounds was found to be significant enough to provide a plausible energetic representation of the complexation and to reveal those differences in the electronic structures of the two complexes which are not obviously seen in the charge density directly.

A more general conclusion to be drawn is the importance of the studies of closely related structures and the usefulness of comparative analyses of static-electronic and thermal parameters. Such efforts can help in interpreting results which are only indirectly deducible from the experiment and must provide a reliable measure of the reproducibility of the method.

Acknowledgment. The authors wish to express their gratitude to Professor H.-B. Bürgi for his criticism and valuable discussions and to Dr. Z. Su and Professor P. Coppens for making their program MOLPROP available. Substantial support of this work by a grant from the Bundesminister für Forschung und Technologie under Contract No. 03-Lu1FUB-OD1-58 is acknowledged, and so is financial assistance by the Fonds der Chemischen Industrie. Finally the authors want to thank Thomas Vogt of ILL, Grenoble, France, for the experimental help.

Supplementary Material Available: Listings of atomic fractional coordinates and anisotropic displacement parameters (2 pages); listing of observed and calculated structure factors (73 pages). This material is contained in many libraries on microfiche, immediately follows this article in the microfilm version of the journal, and can be ordered from the ACS; see any current masthead page for ordering information.